AIChE

Failure of Elastic-Plastic Core–Shell Microcapsules under Compression

Ruben Mercadé-Prieto, Rachael Allen, and Zhibing Zhang
School of Chemical Engineering, University of Birmingham, Birmingham B15 2TT, U.K

David York
Procter and Gamble Technical Centre, Newcastle upon Tyne NE27 0QW, U.K

Jon A. Preece
School of Chemistry, University of Birmingham, Birmingham B15 2TT, U.K

Ted E. Goodwin
ENCAPSYS®, Appleton, P. O. Box 359, Appleton, WI 54912

DOI 10.1002/aic.12804
Published online December 2, 2011 in Wiley Online Library (wileyonlinelibrary.com).

Characterization of the failure behavior of microcapsules is extremely important to control the release of their core actives by mechanical forces. The strain and stress of elastic-plastic uninflated core–shell microcapsules at failure (rupture or bursting) has been determined using finite element modeling (FEM) and micromanipulation compression experiments. The ductile failure of polymeric microcapsules at high deformations is considered to occur when the maximum strain in the shell exceeds a critical strain, resulting in their rupture. FEM has been used to determine the maximum strains present in the capsule wall at different deformations for three types of shell material: elastic, elastic—perfectly plastic and elastic—perfectly plastic with strain hardening at large strains. The results obtained were used to determine the failure strain and stress of melamine-formaldehyde microcapsules, with average population values of ~0.48 and ~350 MPa, respectively. Thus, the elastic-plastic stress–strain relationship has been determined for the core–shell microcapsules tested. © 2011 American Institute of Chemical Engineers *AIChE J,* 58: 2674–2681, 2012
Keywords: failure strain, failure stress, finite element modeling, microcapsule, plasticity

Introduction

Microcapsules with a polymeric or inorganic wall surrounding a core liquid have many applications including the stabilization of functional actives and their controlled release. For example, microcapsules with a perfume oil core are added to laundry detergents to improve the desirable delivery of the perfume to fabrics.[1,2] Understanding the mechanical properties of the microcapsules is crucial for the prediction of their behavior in manufacturing processes and end-use applications. Following the previous example, the microcapsules should be strong enough to survive the washing cycle, but they should also be weak enough to be broken, for example by friction, once they are attached to the fabrics after washing. There are a large number of microcapsules that are designed to release their liquid inner core via the rupture of their shell, unlike in other applications where a continuous release is expected to occur by permeation. Some of these capsules are already commercially available, such as those used in inkless paper,[3] although others are being used to create novel engineering products, for example functional capsules with applications in agrochemicals, washing powders, perfumes and flavors, cosmetics, paints, liquid crystals, pest or mouse repellents, animal feedstuffs, fertilizers, pigments, inks, foaming agents, flame retardants, corrosion inhibitors, mold inhibitors and self-healing polymers.[4] For such applications, characterization of the mechanical strength of microcapsules coupled with an understanding of how it may be controlled by formulation and processing conditions is essential. A detailed understanding on how microcapsules rupture, however, is still scarce.

Rupture information of microcapsules is usually obtained via compression experiments, as reviewed recently by Zhang et al.,[5] whereby single microcapsules are compressed between two parallel plates. Such experiments readily provide the force at which the microcapsule is ruptured or burst,[6] as well as the fractional deformation (compression displacement divided by the capsule diameter) at which it occurs. The rupture force (F_B), and the fractional deformation at rupture (ϵ_B), however, are not intrinsic material properties of the shell, and therefore neither is the nominal rupture stress, which is calculated by dividing F_B by the projected area of the undeformed microcapsule.[7] Nevertheless, these parameters are useful for comparison between different samples prepared under different formulation and processing conditions. The ultimate aim of

Additional Supporting Information may be found in the online version of this article.

Correspondence concerning this article should be addressed to Z. Zhang at Z.Zhang@bham.ac.uk.

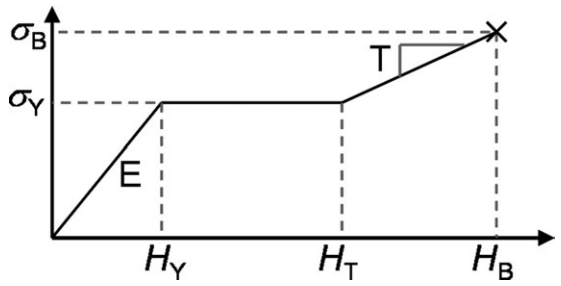

Figure 1. Schematic true stress–strain diagram of an elastic-perfectly plastic material with strain hardening after H_T, with a strain hardening modulus T, until rupture at H_B.

the compression experiments is, however, to be able to determine the stress–strain relationship for the shell deformation up to failure of single microcapsules.

The analysis of the stresses and strains of the shell material while it is being compressed is more complex than typical mechanical tests (e.g., tensile tests), due to the core–shell geometry. Mathematical solutions have been reported in the literature, but usually for the simplest scenarios. Examples include using the thin-shell approximation (no bending resistance),[8,9] hollow spheres,[10] and small deformations,[11] where the shells are fully elastic.[12] In addition, in initially unstressed microcapsules (i.e., not inflated/stretched) there is the additional complexity of the wrinkling of the microcapsule shell in contact with the compression planes.[13] This complexity has prompted the use of finite element modeling (FEM) to simulate the compression of single particles with core–shell structure.[14–16]

Smith et al.[15] were the first to report using FEM to determine the maximum local von Mises stresses and strains in the shell, for inflated fully elastic cells with a core–shell structure similar to microcapsules, at different fractional deformations. As von Mises stresses were considered due to the multiaxial stress conditions, Smith et al.[15] therefore, assumed that the cells are elastic up to bursting and will break at the most stressed/strained region, and so estimated the failure stress (σ_B) and strain (H_B) from the experimental fractional deformation at rupture (ϵ_B) and the elastic modulus (E) of the cell wall. Their results only consider the scenario of cell bursting at high-fractional deformations $\epsilon > 0.4$, where the most stressed/strained region is located at the equator.

Most microcapsules that rupture at such high ϵ_B, however, do not always show elastic behavior. For example, melamine-formaldehyde (MF) core–shell microcapsules, extensively used in industry, are known to behave plastically, at least at fractional deformations $\epsilon > 0.2$, and they may not burst until $\epsilon_B = 0.6$–0.7.[6,7] It has been reported recently[17] that dry MF microcapsules behaved as an elastic-perfectly plastic material, at least up to $\epsilon = 0.5$. Figure 1 shows the schematic true stress — true (Henky) strain diagram of such a material (i.e., the stress and strain using the instantaneous cross-sectional area), where σ_Y is the yield stress and H_Y is the yield strain. When the material is compressed to large strains, strain hardening may occur, as observed in many polymers. A simple case will be considered here, depicted in Figure 1, where strain hardening occurs after H_T with a linear modulus T until rupture at H_B and a rupture stress σ_B.

Once E and σ_Y are known, the determination of H_B and σ_B is the final step for the characterization of the mechanical properties (i.e., the stress–strain diagram) of a shell material with extensive plastic deformation. The failure criterion considered by Smith et al.[15] which states that the shell material will break once the maximum local strain in the shell (H_{max}) exceeds H_B, will also be used in this study. FEM is used here to predict H_{max} at different fractional deformations for a variety of elastic and elastic-plastic scenarios. Note that because the rupture of MF microcapsules occurs after extensive elongation of the shell material, the failure criterion is even more strongly determined by H_{max} than in the elastic scenario of Smith et al.,[15] where the stress could be another reasonable failure criterion. In the perfectly plastic scenario considered here (Figure 1), the stress cannot be used as a failure criterion, only the strain.

Methods

FEM simulations of elastic-plastic capsules using ABAQUS

Single-spherical microcapsules compressed between two parallel plates (a top probe and a bottom substrate), as shown in Figure 2, were simulated using Abaqus 6.5, as described in detail elsewhere.[17–19] Briefly, the capsule shell is simulated as an axisymmetric object in the y plane, with 1440 CAX4RH elements (4-node bilinear, reduced integration with hourglass control, hybrid with constant pressure) and 4 element layers to model the shell for all thicknesses tested (see Figure S1a in the Supplementary Information). The mesh chosen was validated using a much denser mesh, with 20 element layers to model the shell thickness, and a total of 7,200 elements (Figure S1b). Further evidence of the mesh adequacy for a similar problem can be found in Carlisle et al.[20] Different shell thickness h to initial radius r ratios were simulated, between 0.6–9.1%. The liquid core of the microcapsules was designed using FAX2 elements (2-node linear axisymmetric hydrostatic fluid) with a density of 1000 kg m^{-3}. The capsule shell was assumed to be incompressible (Poisson ratio 0.5). Both the

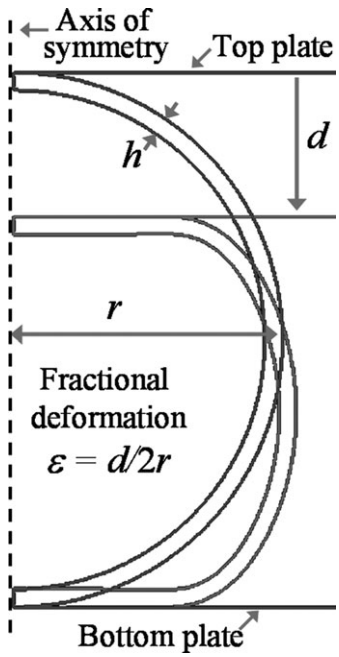

Figure 2. Schematic diagram showing the parallel plate compression of a microcapsule with a liquid core, before and after a displacement d of the top plate.

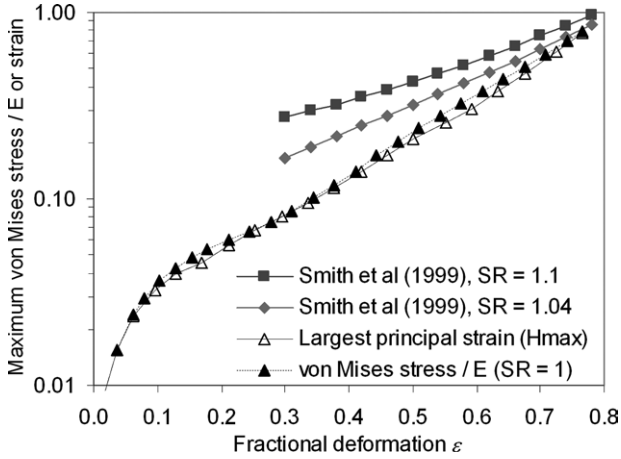

Figure 3. Log-linear plot of maximum von Mises stress (closed symbols) and strain H_{max} (open symbols) in a fully elastic microcapsule (h/r = 0.62%) vs. fractional deformation.

Results from Smith et al.[17] are for inflated core–shell spheres with different initial stretch ratios (SR), shown for comparison.

viscoelasticity and the shell permeability were not considered here for simplicity, as they had been shown to be insignificant in melamine-formaldehyde (MF) microcapsules when compressed within seconds.[6,7] Visco-plasticity was checked by performing compression and holding experiments at high-fractional deformations (Figure S2). Little viscous dissipation was found in the time frame of the compression experiments, therefore, visco-plastic effects were also neglected.

Elastic-perfectly plastic capsules were modeled using a linear elastic material with an elastic modulus E, followed by a plastic regime using classical metal plasticity, where the stress (σ_Y) does not change with plastic strain.[19] Perfect plasticity, the simplest plastic scenario, was found to be appropriate to model the compression behavior of MF microcapsules at $\epsilon < 0.5$,[19] hence, more complex plastic models with more adjustable parameters were not required here. The von Mises yield surface is used to define isotropic yielding. Strain hardening after the perfect plastic regime was modeled as a linear increase of the stress, with a modulus T, after a strain H_T. Simulation results were analyzed to identify the nodes with the highest von Mises stresses and the highest deformations. The values of both E and the initial radius r of the capsules were not relevant due to the use of the dimensionless group F/Erh, and the value of the ratio h/r is important only at small deformations ($\epsilon < 0.2$),[18] whereas different values of σ_Y/E modify the F/Erh profile with ϵ as shown previously.[17]

Melamine-formaldehyde (MF) microcapsules and micromanipulation compressions

The same batch of MF microcapsules as used previously[18] was used here for consistency, with hexyl salicylate oil as the liquid core. A diluted water suspension with the MF microcapsules was dropped onto a glass substrate and the water was evaporated by incubation of the substrate in an oven at 353 K for 600 s. The glass substrate with the dry microcapsules was then placed on a stage of a micromanipulation rig to perform the compressions. Single microcapsules were compressed between two flat surfaces, described in detail elsewhere.[5,21] Three force transducers (two models 403A and one model 405A, Aurora Scientific, Inc., Canada) were used with different mounted probes (ϕ ~26 μm, ~45 μm and ~99 μm) to compress microcapsules of 4– 40 μm in diameter, at a compression speed of 2.4 μm s^{-1} for small microcapsules (<20 μm), and 4 μm s^{-1} for larger ones.

Results and Discussion

FEM: elastic shell

The simplest scenario of a microcapsule shell with elastic behavior is considered first, as a continuation of the research of Smith et al. on inflated elastic spheres with core–shell structure (e.g., yeast cells).[22] Their results are given as a dimensionless stress, where the maximum von Mises stress found at each fractional deformation is multiplied by the initial stretch ratio (which in this case is one), and divided by the elastic modulus (E) and the ratio of initial shell thickness to radius (h/r). In their analysis they did not carry out simulations with different h/r values and, hence, they did not appreciate that the correct dimensionless group should not incorporate h/r: it is simply the maximum von Mises stress/E (for uninflated core–shell spheres) as shown in Figure S3 (Supplementary Information). Figure 3 compares these results with those reported by Smith et al. for two initial stretch ratios (SR), where it is obvious that our results for SR = 1 are smaller than those for the latter cases. For the subsequent results on elastic-perfectly plastic shells, however, the maximum von Mises stress is not useful in determining the failure criterion and the critical parameter to report is the maximum strain, as mentioned previously. As a result of the multiaxial stress conditions both normal and shear strains are not equal to zero. As the aim is to obtain a single critical strain that can be used to quantify the rupture of the microcapsule, the principal strains were considered (refer to the Supplementary Information).[23] Two of the principal strains are in the 2-D (two-dimensional) plane shown in Figure 2, although the third is normal to that plane (termed out-of-plane). All three principal strains along the shell are not equal to zero (unlike in a typical tensile test). For simplicity, results will show the largest absolute principal strain value found in the shell, termed H_{max}. In the elastic scenario, H_{max} is very similar to the maximum von Mises stress/E as expected, as shown in Figure 3.

Due to the large variation of the shell thickness in different microcapsules, the effect of h/r on H_{max} was investigated by FEM and the results are in shown in Figure 4a. Details on the nature of the most strained nodes in the FEM are illustrated in Figures S5 and S6 (Supplementary Information). Figure 4b shows the position in the undeformed shell of these nodes, where 0° corresponds to the equator, and 90° to the top/bottom of the capsule. At large fractional deformations (ϵ), the most strained (and stressed) region is at the equator, as reported previously.[22] At $\epsilon > 0.6$, the largest strain is the minimum in-plane strain, caused by the thinning of the shell thickness (Figure S5b and e). At $0.3 < \epsilon < 0.6$ the largest strain is the out-of-plane strain, resulting from the stretching along the meridian (Figure S5c), and its position differs from the equator at ϵ lower than ~0.45 (Figure 4b). Note that for $\epsilon > 0.3$, the value of h/r has little effect on the maximum true strain (the same is observed in stress terms in Figure S3a), as the main deformation mode is the stretching of the shell. At lower fractional deformations ($\epsilon < 0.3$), bending effects become important in thicker shells, resulting in different stresses and strains at equal ϵ for different h/r shells. In thick shells (e.g., $h/r > 4\%$) the most strained region is that in contact with the probe/substrate, where

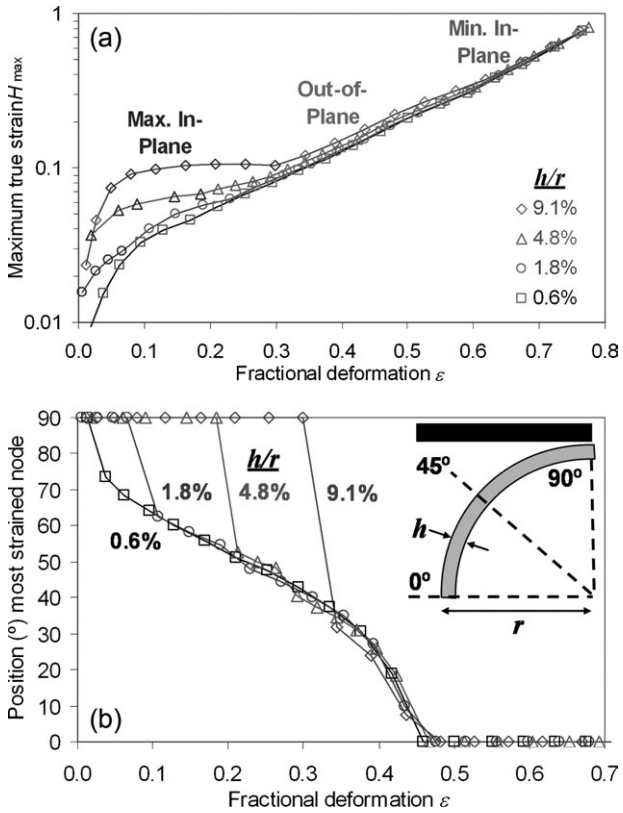

Figure 4. (a) Log-linear plot of maximum true strain H_{max} for fully elastic microcapsules with 4 different h/r values vs. fractional deformation.

The color of the points indicates the largest plane strain: Maximum in-plane (blue), out-of-plane (red), or minimum in-plane (green), and (b) position of the most strained nodes shown in the inset sketch using the undeformed shape of a capsule (top left cross section of a microcapsule with the compressing probe on top).

wrinkling occurs.[13] Wrinkling causes compression of the external face of the shell. This compression in the shell-surface plane leads to expansion in the transverse direction, which is given by H_{max} shown in Figure 4a as maximum in-plane strain (Figure S5a and d). For thin shells and small deformations (e.g., $h/r = 0.6\%$ and $\epsilon < 0.2$), the largest strain is usually caused by compression in the longitudinal direction of the inner side of the shell in the area of greatest bending (its position is shown in Figure 4b).

FEM: Elastic-perfectly plastic shell

In order to guarantee ductile failure of the capsule, there must be extensive yielding prior to failure. For typical values between 0.012–0.07 of the yield stress to elastic modulus ratio (σ_Y/E), the fractional deformation should be higher than ~0.3.[17] Although ductile failure can certainly occur at lower ϵ values, it will be difficult to ascertain from compression force data alone. By focusing only on $\epsilon > 0.3$, the complex behavior of H_{max} at different h/r values, previously discussed for the fully elastic scenario, can be obviated.

Figure 5 shows the strain composition of the most strained nodes from simulations corresponding to three different σ_Y/E values. For $\epsilon = 0.3$–0.5, the out-of-plane strain is again the largest, and there is no effect of σ_Y/E on H_{max}, agreeing with the fully elastic results. Note that as elasticity and perfect-plasticity are the most extreme constitutive models, all other plastic models (i.e., isotropic hardening) fall between these two, at the same deformation. Hence, at $\epsilon < 0.5$, H_{max} for any other plastic stress–strain relationship can still be calculated with these results using the fully elastic- or elastic-perfectly plastic results.

The position of the most strained node moves to the equator faster than in the elastic scenario (inset Figure 5). At $\epsilon > 0.5$, H_{max} for the elastic-perfectly plastic shells increases much faster than the elastic cases, and the lower the σ_Y/E value, the faster the increase. There is a point, $\epsilon = 0.55$–0.6, where the shell thickness at the equator is reduced so quickly that the FEM software fails to find reasonable solutions (Figure S7). The very strained area of the equator appears wrinkled, and the continuity of many parameters such as the compression force is not maintained at that point, indicating that the simulation results are not correct. It is unlikely that this problem was induced by the simulations, since using finer meshes was equally unsuccessful. This phenomena may result from extensive deformation without resistance (perfect plasticity) occurring at the equator area, which requires further investigation.

The H_{max} of many simulations performed for the elastic and elastic-perfectly plastic scenarios with different shell thickness to radius ratios and yield stress to elastic modulus ratios are summarized in Figure 6. Although h/r and σ_Y/E have some effects on H_{max}, they are small and can be obviated when determining an average correlation between H_{max} and the fractional deformation, given in Figure 6.

FEM: elastic-perfectly plastic with strain hardening shell

Although an elastic-perfectly plastic model can satisfactorily explain, in a simple manner, the stress–strain behavior of many polymers at small strains, it is not reasonable to expect that the stress will remain invariant at large deformations. Strain hardening at large deformations (usually at strains H_T larger than ~0.3–0.5) is known to occur in the case of many plastic polymers, such as polypropylene,[24] polyethylene,[25] PMMA,[26] or polycarbonate.[27] Strain hardening solves, incidentally, the FEM

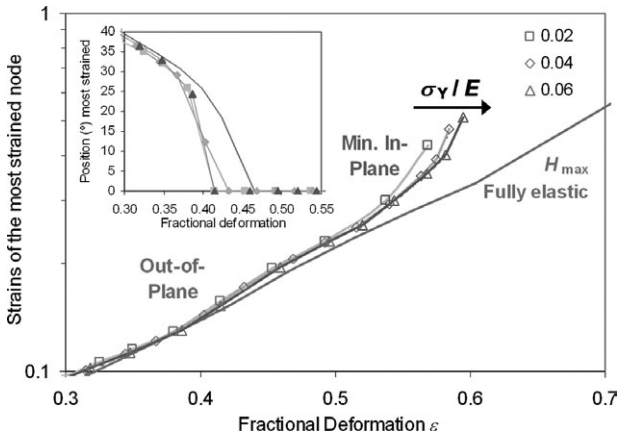

Figure 5. Log-linear plot of plane strains of the most strained nodes for a h/r = 4.8% elastic-perfectly plastic microcapsule with σ_Y/E = 0.02 (squares), 0.04 (diamonds), and 0.06 (triangles) vs. fractional deformation.

Continuous lines represent H_{max}, the largest of the three plane strains at each fractional deformation. H_{max} for the fully elastic scenario is shown for comparison. Inset shows the position of the most strained nodes as described in Figure 4b.

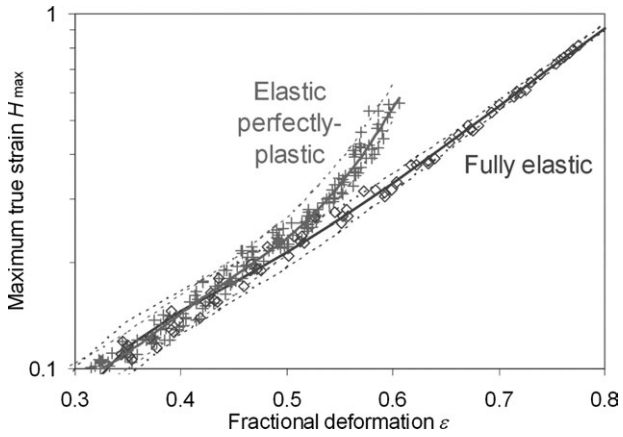

Figure 6. Log-linear plot of maximum strains determined from FEM of fully elastic and elastic-perfectly plastic capsules vs. fractional deformation.

For the former, results from six simulations with h/r between 0.6 and 9.1% are shown. Elastic—perfectly plastic results comprise 21 simulations with h/r between 0.6 and 9.1% and σ_Y/E between 0.012 and 0.07. Continuous lines are best-fit polynomials; dashed lines are the 95% confidence interval (CI) of the fitted equations. Fully elastic: $H_{max} = 7.87\epsilon^3 - 9.26\epsilon^2 + 4.21\epsilon - 0.563$ (± 0.02; 95% CI), Elastic perfectly-plastic: $H_{max} = 454.3\epsilon^5 - 845.8\epsilon^4 + 620.9\epsilon^3 - 222.51\epsilon^2 + 39.07\epsilon - 2.621$ (± 12%; 95% CI).

problem at $\epsilon > 0.55$ mentioned previously, suggesting that it was caused by a plastic collapse. For simplicity, a linear strain-hardening behavior, described with a strain hardening modulus T has been considered (Figure 1). Figure 7 shows the compression force profile both with and without strain hardening for two values of the ratio T/E with $H_T = 0.25$.

There are now 4 parameters available to perform the simulations: h/r, σ_Y/E, H_T and T/E. Note, however, that it is possible to eliminate the first two by considering that when $\epsilon = 0.3$–0.45, the dimensionless group F/Erh is linearly dependent on σ_Y/E and almost independent of h/r.[17] Hence, a "plastic" master plot can be constructed considering the dimensionless group $F/\sigma_Y rh$ instead of F/Erh. In such a plot (shown in Figures 8 and S8) all curves overlap during the

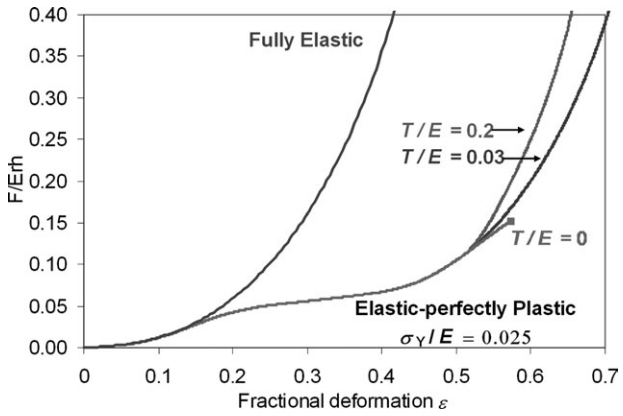

Figure 7. Dimensionless force profiles with the fractional deformation for a microcapsule with h/r = 1.2% and different shell material properties: fully elastic, elastic-perfectly plastic without (T/E = 0) and with strain hardening (T/E > 0) after H_T = 0.25.

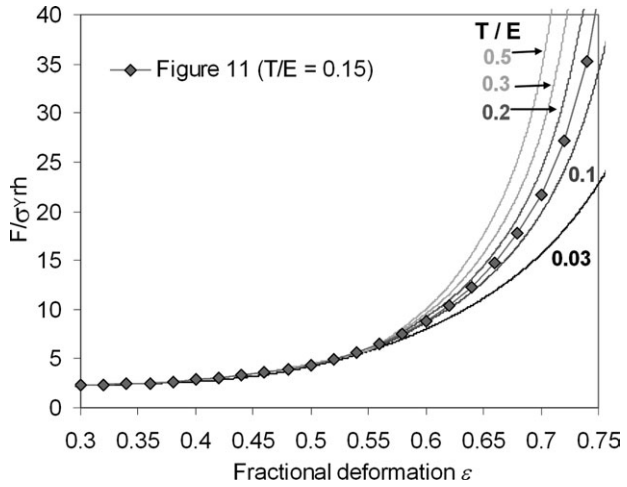

Figure 8. Effect of the strain hardening modulus ratio T/E (0.03–0.5) on the dimensionless force group normalized with the yield stress.

Points are the results for the conditions of Figure 11, with the following best-fitted equation: $F/\sigma_Y rh = 1.945 + 1.12 \times 10^{-15}\exp(48.5\epsilon) + 0.0143\exp(10.29\epsilon)$ for $0.3 < \epsilon < 0.75$.

plastic stage ($\epsilon = 0.3$–0.45), and they obviously deviate at smaller fractional deformations ($\epsilon < 0.3$). Deviations at high deformations are, thus, caused only by H_T and T/E. Figure 9 shows the effect of strain hardening on the estimated H_{max}, with the two different T/E values used in Figure 7. The resulting data deviates from the elastic-perfectly plastic scenario when $H_{max} > H_T$, and, thereafter, tends to follow the fully elastic scenario. The T/E value does affect the determined H_{max} at high ϵ, and higher T/E results in lower H_{max}.

Determination of the failure parameters from experimental compression data

We have reported previously that dry melamine-formaldehyde (MF) microcapsules with hexyl salycilate core behaved as an elastic -perfectly plastic material at $\epsilon < 0.5$.[17] Here the compression force profiles will be described fully until bursting. Approximately 150 compressions were performed on microcapsules of 4–40 μm in diameter. Figure 10a shows the typical linear correlation found between the bursting force and the capsule size,[6] with an average $F_B/2r$ of 240 ± 60 (SD) N m^{-1}. A linear correlation is expected if the capsule failure under such stretched conditions occurs at a specific fractional deformation, which is considered to be determined by H_B of the shell material. Using the master plot of Figure 8, if the fractional deformation at rupture is unique and $\sigma_Y h$ does not change with the capsule size, then the ratio of the bursting force to the capsule size will also be a constant. The product $\sigma_Y h$ is determined for each individual experiment using Figure 8 for $\epsilon = 0.3$–0.45 (see Figure 10b), and has the average value of 27 ± 7 N m^{-1}. As can been seen, the population variability of $\sigma_Y h$ is much higher than the standard error of each determination, which may be due to the variability of σ_Y and h. Regarding the latter, we have shown previously that the wall thickness h of the microcapsules,[18] despite being independent of the capsule size, also has a significant variability of ~25%. Theoretically speaking, σ_Y can also vary between microcapsules even if they have same size, since microcapsules result from the deposition of melamine formaldehyde on the surface of the oil droplets, which had been continuously exposed to

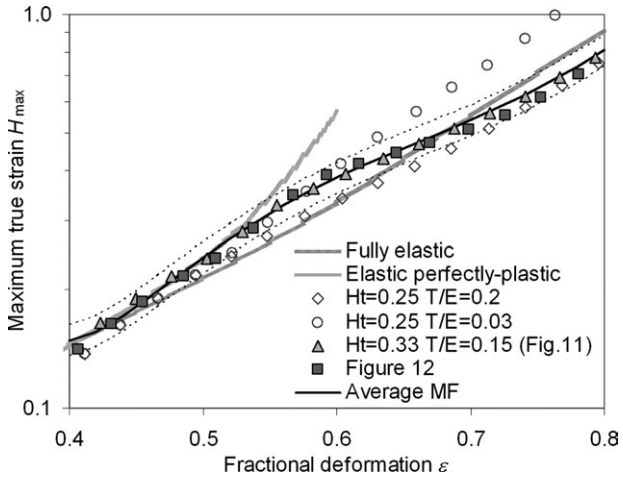

Figure 9. Log-linear plot of maximum true strain H_{max} for microcapsules with strain hardening vs. fractional deformation.

Open symbols are two examples with very little (T/E = 0.03, circles) or significant (T/E = 0.2, diamonds) strain hardening. Filled triangle and square points are determined from the simulations of Figures 11 and 12, respectively. Continuous black line is the best-fit correlation for the fitted MF microcapsules: $H_{max} = 6.061 - 44.18\epsilon + 119.12\epsilon^2 - 138.04\epsilon^3 + 59.88\epsilon^4$ (±10%; 95% CI). Dashed lines represent the 95% CI of simulations used to fit the experimental force data.

hydrodynamic forces generated in a stirred vessel (see Methods section). Nevertheless, there is no discernible trend between $\sigma_Y h$ and the capsule size. The elastic regime was also calculated as described in the literature,[18] resulting in an average Eh of 780 ± 300 N m^{-1} (Figure S9). For a shell thickness value of ~0.185 μm,[18] the average population values of E and σ_Y are 4.2 ± 2 GPa and 150 ± 40 MPa, respectively. Note that the value of the bursting force is of little use for plastic microcapsules. As a self-consistency check, the experimental average $F_B/2r$ can be used with the equation in Figure 8 and the mean ϵ_B to verify the yield stress of the shell material.

The elastic modulus and the yield stress are readily calculated for individual compression experiments. A similar approach for determination of the strain hardening parameters could be considered, but is very time-consuming, and not recommended. For reasons that are detailed in the Supplementary Information, there is a significant uncertainty at high deformations. For example, for a microcapsule with a nominal fractional deformation at rupture ϵ_B of 0.68, a 3.3% uncertainty of the capsule size (e.g., 0.5 μm for a 15 μm capsule) leads (*ceteris paribus*) to an uncertainty of ϵ_B by ±0.023. Yet, a capsule that breaks at ϵ = 0.657 will result in an estimated T/E much higher than if it breaks at 0.703, and T/E would be 0.2 and 0.03, respectively, with the conditions in Figure 7. This fitting is based on the assumption that H_T can also be accurately determined. Therefore, an optimization process to find the best fit of H_T and T/E, using FEM data, is unreasonable at present, and would obviate the fact that Figure 1 is already a simplification.

First, ϵ_B ought to be determined as accurately as possible. However, an independent determination of ϵ_B from the compression force profiles can only be made from video recordings of compression experiments just before bursting when large particles are used (>20 μm). Direct measurements on video recordings show that they burst at ϵ_B approximately ~0.65–0.70. More precise measurements can be obtained by measuring the extension at the equator, which is 0.490 ± 0.015 (SD, n = 10) corresponding to a ϵ_B of 0.672 ± 0.008 (see Figure S10). These values agree well with the ϵ_B determined from the force profiles of large capsules (20–40 μm), i.e., 0.68 ± 0.03 (n = 25). For smaller capsules, a value of 0.70 ± 0.04 is found, which is not statistically different (p = 0.02) from the larger ones.

Once the fractional deformation at rupture was verified to be around 0.68, H_T and T/E were determined heuristically by comparing the FEM dimensionless force profiles with the experimental data. Figure 11 shows the compression of six different MF microcapsules with very similar properties: r, Eh, $\sigma_Y h$ and ϵ_B. The continuous line is the analogous elastic–perfectly plastic with strain hardening simulation with H_T = 0.33 and T/E = 0.15. Figure 9 shows the determined H_{max} under these strain hardening conditions, resulting in $H_{max} = H_B$ ~0.49 at the rupture and ϵ_B ~0.68. The rupture stress σ_B is finally determined using σ_Y, H_T, H_B and T, which is ~325 MPa. The complete stress–strain diagram estimated for the shell material can now be constructed as shown in Figure 11 (inset).

The experimental accuracy of ϵ_B for an individual compression was estimated to be ±0.026 (refer to the Supplementary

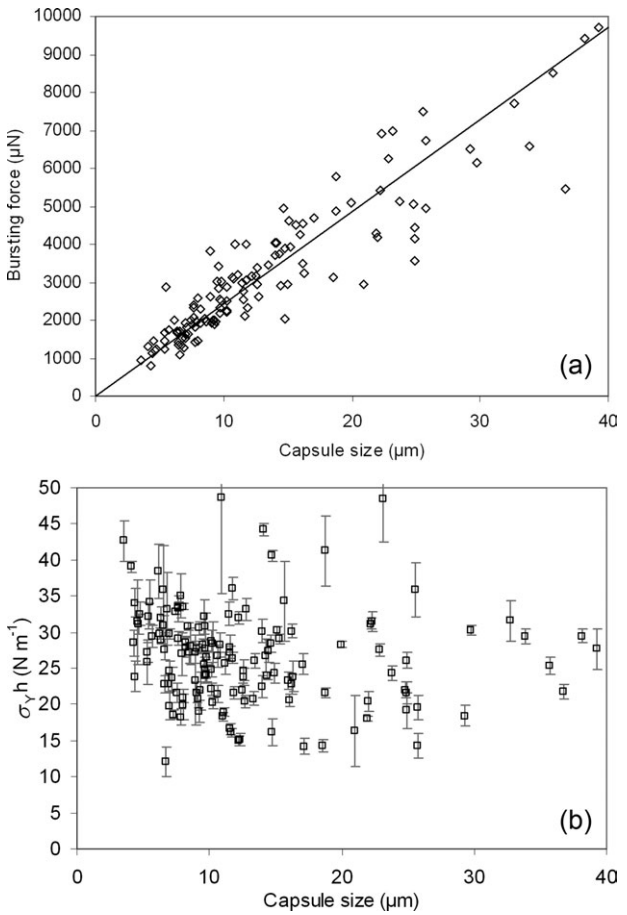

Figure 10. (a) Bursting force of melamine-formaldehyde (MF) microcapsules of different size, and (b) estimated $\sigma_Y h$ for each individual compression using Figure 7 at 4 points between ϵ 0.3–0.45.

The error bars show the standard deviation (SD) of the four estimates.

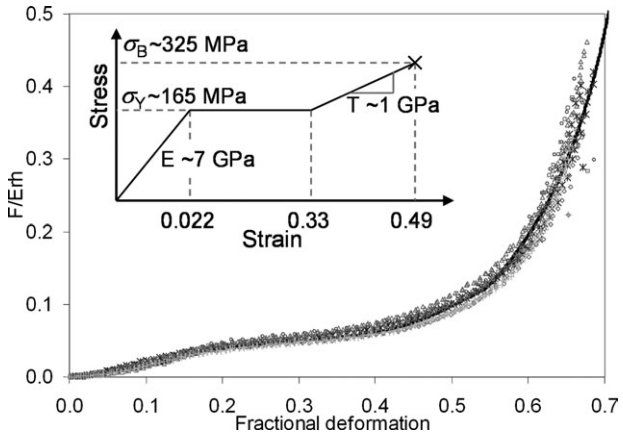

Figure 11. Experimental compression curves of 6 different melamine-formaldehyde microcapsules (r = 2.5–6 μm, Eh ~1300 N m^{-1} and $\sigma_Y h$ ~30 N m^{-1}).

Continuous line is the FEM results for an elastic-perfectly plastic with strain hardening microcapsule, using h/r = 4.8%, σ_Y/E = 0.022, H_T = 0.33 and T/E = 0.15. Inset shows the predicted stress–strain relationship of the MF shell using h = 0.185 μm.

Information). A sensitivity analysis was conducted on several examples to determine the corresponding uncertainty of the failure and strain hardening parameters. The nominal capsule size was modified in order to vary the calculated ϵ_B by $\pm$0.026. New T values were calculated using FEM for the modified force profiles (H_T was kept at 0.33 for simplicity); Table 1 shows the results of one example. H_{max} was then calculated from each FEM simulation at the 3 ϵ_B values (note that H_{max} is reduced at higher T values, see Figure 9), which allows determination of σ_B. The experimental uncertainty of ϵ_B yields an estimated error of ~15% for both failure parameters. A similar error estimate for H_{max} (and thus H_B) can be obtained using the average correlation presented in Figure 9, and the values are shown in Table 1, without the need to perform additional simulations. Some estimates of T are required, however, for example using Figure 8, in order to determine the error of σ_B in this simpler way.

More complex strain hardening scenarios

Some experimental compression profiles at high deformations could not be well described using a single linear strain hardening modulus T. FEM simulations were performed by considering two linear strain hardening moduli, and fitting its parameters heuristically, in order to verify their effect on the determined H_B and σ_B. One example is shown in Figure 12; the determined H_{max} at those conditions is shown in Figure 9. Despite the different strain hardening scenarios, the predicted H_B is very similar, i.e., ~0.47 (with ϵ_B ~0.66). In fact, all the different strain hardening scenarios tested and optimized to the different individual experimental compressions, resulted in H_B values that agree within $\pm$0.05, which is in the same order as the error estimated for an individual measurement.

Table 1. Sensitivity Analysis of the Estimated Uncertainty of ε_B in the Determination of the Strain Hardening Modulus T, and how Both Affect the Failure Strain (H_B) and Stress (σ_B)

ε_B	T (MPa)	H_B	σ_B (MPa)
Initial +0.026	~800	0.52 (0.53)†	330 (340)‡
Initial	~1500	0.44 (0.46)†	360 (390)‡
Initial -0.026	~4000	0.39 (0.42)†	405 (570)‡

Values in brackets are calculated using:
†the correlation given in Figure 8;
‡the bracketed H_B values.

The elastic-perfectly plastic model, with strain hardening at large strains, is an acceptable simplification of the real stress–strain relationship observed in many polymers.[24;26] It has been chosen in this work because it is the simplest plasticity scenario, and fits the experimental data well, but it cannot be claimed to be the optimal. Using different elastic-plastic models to fit the experimental data for the reverse engineering problem, such as the case in this work, is time-consuming if not impossible. Nevertheless, the model used in this case is the simplest, and the obtained failure parameters are, therefore, useful in the comparison of the mechanical strength of microcapsules prepared using different formulation and processing conditions, particularly when the model is representative of the material behavior (in this case elastic, elastic-perfectly plastic, and elastic-perfectly plastic with strain hardening). If, in some cases, the shell does not show perfect plasticity, e.g., isotropic hardening, the H_{max} results of Figure 6 are still valid up to $\epsilon < 0.5$ since it can be seen that there is no significant difference in H_{max} between the two extreme models (elastic and elastic-perfectly plastic). Therefore, determination of the strain at rupture H_B (but not σ_B) is possible, which can still be used to identify how the formulation and processing conditions may affect the failure parameter. Models to estimate H_B corresponding to $\epsilon > 0.5$ and σ_B for non-perfect plastic shell materials shall be developed in the future, but at present there is not sufficient experimental data to justify it.

Conclusions

FEM simulations have been performed on uninflated core–shell microcapsules compressed between two parallel plates. At fractional deformations higher than 0.3, the largest strains are caused by the out-of-plane stretching in the meridian direction and by the thinning of the shell thickness. The equator region,

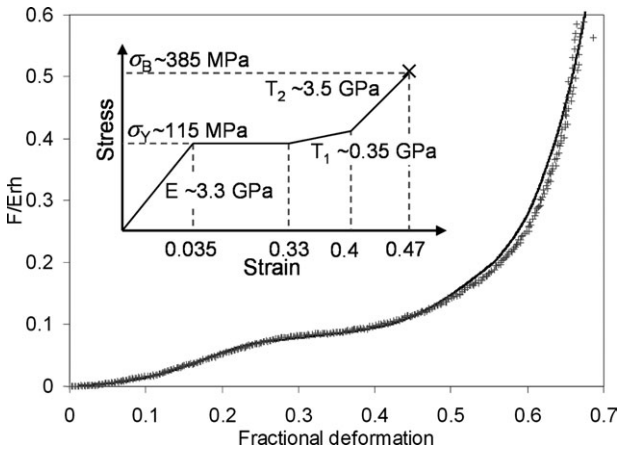

Figure 12. Example of a compression profile fitted using two strain hardening moduli.

Experimental points are for a microcapsule with r = 8.5 μm, Eh = 620 $\pm$ 90 N m^{-1} and $\sigma_Y h$ = 21 $\pm$ 1 N m^{-1}). Continuous line is the FEM simulation with h/r = 3.2%, σ_Y/E = 0.035, H_{T1} = 0.33, T_1/E = 0.1, H_{T2} = 0.4 and T_2/E = 1. Inset shows the predicted stress–strain relationship of the MF shell using h = 0.185 μm.

the most strained part of the shell at high deformations, of elastic-perfectly plastic shells only becomes more strained than the fully elastic scenario at $\epsilon > 0.5$. Thereafter, the shell thickness thins very quickly, resulting in the probable failure of the FEM. Strain hardening after the perfectly plastic regime was included, solving this modeling problem, and providing a more realistic material model for plastic polymers. The whole compression profile of melamine-formaldehyde microcapsules up to bursting was modeled for the first time using an elastic-perfectly plastic model with strain hardening. Reasonable estimates of the strain hardening parameters are only required to obtain consistent strain values at rupture H_B, found to be $\sim$0.48 for MF microcapsules. The failure stress σ_B was estimated to be $\sim$350 MPa. The uncertainty of H_B and σ_B are mostly determined by the accuracy of fractional deformation at rupture (ϵ_B). Future work will investigate the mechanical strength of microcapsules prepared using different formulation and processing conditions, including FEM based on different elastic-plastic models.

Acknowledgments

The authors gratefully acknowledge financial support from the Engineering and Physical Sciences Research Council (EPRSC), U.K., through grant number EP/F068395/1. Some of the equipment used in this research were obtained, through Birmingham Science City: Innovative Uses for Advanced Materials in the Modern World (West Midlands Centre for Advanced Materials Project 2), with support from Advantage West Midlands (AWM) and part funded by the European Regional Development Fund (ERDF).

Notation

d = top-plate displacement, m
E = elastic modulus, Pa
F = compression force, N
F_B = compression force at rupture, N
h = shell thickness, m
H = true (Henky) strain
H_B = true strain at rupture
H_{max} = largest plane strain in the capsule shell
H_T = true strain where strain hardening starts
H_Y = true strain at the yield point
r = initial capsule radius, m
SR = initial stretch ratio
T = strain hardening modulus, Pa

Greek letters

ϵ = fractional deformation
ϵ_B = fractional deformation at rupture
σ = true stress, Pa
σ_B = true stress at rupture, Pa
σ_Y = yield stress, Pa

Literature Cited

1. Long Y, Vincent B, York D, Zhang ZB, Preece JA. Organic-inorganic double shell composite microcapsules. *Chem Commun*. 2010;46:1718–1720.
2. Long Y, York D, Zhang ZB, Preece JA. Microcapsules with low content of formaldehyde: preparation and characterization. *J Mater Chem*. 2009;19:6882–6887.
3. Yow HN, Routh AF. Formation of liquid core-polymer shell microcapsules. *Soft Matter*. 2006;2:940–949.
4. Caruso MM, Blaiszik BJ, Jin HH, Scheikopf SR, Stradley DS, Sottos NR, White SR, Moore JS. Robust, double-walled microcapsules for self-healing polymeric materials. *Acs Appl Mater Interface*. 2010;2:1195–1199.
5. Zhang Z, Stenson JD, Thomas CR. *Chapter 2 micromanipulation in mechanical characterisation of single particles*. In: Jinghai L, ed. *Advances in Chemical Engineering, Characterization of Flow, Particles and Interfaces*. Academic Press; 2009;29–85.
6. Sun G, Zhang Z. Mechanical properties of melamine-formaldehyde microcapsules. *J Microencap*. 2001;18:593–602.
7. Hu JF, Chen HQ, Zhang ZB. Mechanical properties of melamine formaldehyde microcapsules for self-healing materials. *Mater Chem Phys*. 2009;118:63–70.
8. Lardner TJ, Pujara P. Compression of spherical cells. *Mech Today*. 1980;5:161–176.
9. Stenson JD, Thomas CR, Hartley P. Modelling the mechanical properties of yeast cells. *Chem Eng Sci*. 2009;64:1892–1903.
10. Gregory RD, Milac TI, Wan FYM. A thick hollow sphere compressed by equal and opposite concentrated axial loads: An asymptotic solution. *SIAM J Appl Math*. 1999;59:1080–1097.
11. Wan KT, Chan V, Dillard DA. Constitutive equation for elastic indentation of a thin-walled bio-mimetic microcapsule by an atomic force microscope tip. *Colloids Surf B*. 2002;27:241–248.
12. Liu KK. Deformation behaviour of soft particles: a review. *J Phys D Appl Phys*. 2006;39:R189–R199.
13. Nadler B. On the contact of a spherical membrane enclosing a fluid with rigid parallel planes. *Int J Non Linear Mech*. 2010;45:294–300.
14. Nguyen VB, Wang CX, Thomas CR, Zhang Z. Mechanical properties of single alginate microspheres determined by microcompression and finite element modelling. *Chem Eng Sci*. 2009;64:821–829.
15. Smith AE, Moxham KE, Middelberg APJ. On uniquely determining cell-wall material properties with the compression experiment. *Chem Eng Sci*. 1998;53:3913–3922.
16. Rachik M, Barthes-Biesel D, Carin M, Edwards-Levy F. Identification of the elastic properties of an artificial capsule membrane with the compression test: Effect of thickness. *J Colloid Interface Sci*. 2006;301:217–226.
17. Mercadé-Prieto R, Allen R, York D, Preece JA, Goodwin TE, Zhang Z. Compression of elastic -perfectly plastic microcapsules using micromanipulation and finite element modelling: Determination of the yield stress. *Chem Eng Sci*. 2011;66:1835–1843.
18. Mercadé-Prieto R, Nguyen B, Allen R, York D, Preece JA, Goodwin TE, Zhang Z. Determination of the elastic properties of compressed microcapsules using finite element modelling. *Chem Eng Sci*. 2011;66:2042–2049.
19. ABAQUS. *Analysis User's Manual, Version 6.5*. Hibbit, Karlsson and Sorensen, Inc.; 2005.
20. Carlisle KB, Lewis M, Chawla KK, Koopman M, Gladysz GM. Finite element modeling of the uniaxial compression behavior of carbon microballoons. *Acta Mater*. 2007;55:2301–2318.
21. Zhang Z, Ferenczi MA, Lush AC, Thomas CR. A novel micromanipulation technique for measuring the bursting strength of single mammalian-cells. *Appl Microbiol Biotechnol*. 1991;36:208–210.
22. Smith AE, Moxham KE, Middelberg APJ. Wall material properties of yeast cells. Part II. Analysis. *Chem Eng Sci*. 2000;55:2043–2053.
23. Gere JM, Goodno BJ. *Analysis of stress and strain*. In: *Mechanics of Materials*. 7th ed. Toronto, Canada: Cengage Learning; 2009; 536–618.
24. Michaeli W, Glissmann M. Investigation and measurement of the true stress/strain behaviour of semi-crystalline thermoplastics. *Macromol Mater Eng*. 2000;284:19–24.
25. Hiss R, Hobeika S, Lynn C, Strobl G. Network stretching, slip processes and fragmentation of crystallites during uniaxial drawing of polyethylene and related copolymers. A comparative study. *Macromolecules*. 1999;32:4390–4403.
26. Arruda EM, Boyce MC, Jayachandran R. Effects of strain rate, temperature and thermomechanical coupling on the finite strain deformation of glassy polymers. *Mech Mater*. 1995;19:193–212.
27. Stachurski ZH. Deformation mechanics and yield strength in amorphous polymers. *Progr Polym Sci*. 1997;22:407–474.

Manuscript received Apr. 6, 2011, and revision received Oct. 8, 2011.